Accepted Manuscript

Structural and electrochemical properties of the $Li_2FeP_2O_7$/C composite prepared using soluble methylcellulose

Dragana Jugović, Miodrag Mitrić, Miloš Milović, Valentin N. Ivanovski, Srečo Škapin, Biljana Dojčinović, Dragan Uskoković

PII: S0925-8388(19)30431-1

DOI: https://doi.org/10.1016/j.jallcom.2019.01.392

Reference: JALCOM 49430

To appear in: *Journal of Alloys and Compounds*

Received Date: 20 November 2018

Revised Date: 18 January 2019

Accepted Date: 31 January 2019

Please cite this article as: D. Jugović, M. Mitrić, Miloš. Milović, V.N. Ivanovski, Sreč. Škapin, B. Dojčinović, D. Uskoković, Structural and electrochemical properties of the $Li_2FeP_2O_7$/C composite prepared using soluble methylcellulose, *Journal of Alloys and Compounds* (2019), doi: https://doi.org/10.1016/j.jallcom.2019.01.392.

Structural and electrochemical properties of the $Li_2FeP_2O_7$/C composite prepared using soluble methylcellulose

Dragana Jugović[a,*], Miodrag Mitrić[b], Miloš Milović[a], Valentin N. Ivanovski[b], Srečo Škapin[c], Biljana Dojčinović[d], and Dragan Uskoković[a]

[a]Institute of Technical Sciences of SASA, Knez Mihailova 35/IV, 11 000 Belgrade, Serbia

[b]University of Belgrade, Vinča Institute of Nuclear Sciences, P.O. Box 522, 11 001 Belgrade, Serbia

[c]Jožef Štefan Institute, Jamova 39, SI-1000 Ljubljana, Slovenia

[d] University of Belgrade, Institute of Chemistry, Technology and Metallurgy, Njegoševa 12, 11000 Belgrade, Serbia

Abstract

A new method involving the homogeneous dispersion of precursor compounds inside a methylcellulose matrix is used for the synthesis of a composite powder of $Li_2FeP_2O_7$ and carbon. The properties of carbon-containing and carbon-free powders are studied by X-ray powder diffraction (XRD) including Rietveld refinement, Mössbauer spectroscopy, Fourier transform infrared spectroscopy (FTIR), field emission scanning electron microscopy (FESEM), galvanostatic cycling, and electrochemical impedance spectroscopy (EIS). The structure of both powders is refined in a monoclinic framework (space group $P2_1/c$). The structural refinement and Mössbauer spectroscopy reveal different degrees of partial occupancy of mixed-occupied sites

by lithium. Electrochemical measurements show that the *in situ* formation of carbon improves capacity (90% of 1-electron theoretical capacity) through decreased charge-transfer resistance.

Keywords: Energy storage materials; Crystal structure; Electrochemical reactions; X-ray diffraction; Mössbauer spectroscopy

*Corresponding author:

Dr Dragana Jugović

Institute of Technical Sciences of SASA, Knez Mihailova 35/IV, 11000 Belgrade, Serbia

Phone: +381 64 1177549

e-mail: dragana.jugovic@itn.sanu.ac.rs; djugovic@vinca.rs

1. Introduction

The interest in polyanion cathode materials for lithium-ion batteries is rising because they operate at higher voltages and ensure better safety than their oxide counterparts with the same $M^{2+/3+}$ redox pair. The crystal structure and covalency of the polyanion affect the $M^{2+/3+}$ redox energies in polyanion cathodes [1]. Different crystal structures of $LiFePO_4$, Li_2FeSiO_4, $Li_2FeP_2O_7$, and $LiFeBO_3$ have different redox energies. Among them, $LiFePO_4$ is the most widely studied polyanion cathode material and it has already been commercialized. However, there is an interest in finding new polyanion cathode materials that would a have higher voltage vs. Li/Li^+ than $LiFePO_4$ [2]. $Li_2FeP_2O_7$ has a somewhat higher voltage than $LiFePO_4$ (3.5 and 3.4

V, respectively) and it also enables two-electron reactions, where the theoretical capacity could reach 220 $mAhg^{-1}$ nearing the capacity of some oxides [3,4]. Its structure consists of corner-shared dimers of PO_4 tetrahedra (P_2O_7 units) interconnected with FeO_6 octahedra and FeO_5 trigonal bipyramids [5]. Contrary to isostructural lithium manganese pyrophosphate ($Li_2MnP_2O_7$), the structure of $Li_2FeP_2O_7$ reveals both Li and Fe mixed site occupancies due to an additional mixed-occupied site for iron and an additional mixed-occupied site for lithium. An anti-site defect is found to be the most favourable defect, particularly for these mixed-occupied sites [6]. Atomistic modelling techniques predict high Li^+ mobility along the *b*-axis and *c*-axis channels that form a quasi-two-dimensional (2D) Li migration in the *bc*- plane [6]. Under the condition of partial occupancy by lithium and transition metal atoms, the fifth lithium mixed-occupied site can mediate Li^+ ion diffusion between two-dimensional Li^+ ion pathways, transforming Li^+ ion pathways into a 3D network [7].

So far, $Li_2FeP_2O_7$ or its composites with carbon have been synthesized in various ways, such as the conventional solid-state method [8–12], mechanochemically assisted solid state synthesis [13], combustion method [14], sol-gel method [15], spray pyrolysis [16], etc. The solid-state method is widely adopted in industry for the mass production of cathode materials due to its simplicity and low cost. It is also suitable for simultaneous carbon coating during powder synthesis by introducing an organic compound in a precursor mixture. Coating with electronically conductive agent (usually carbon) is extensively utilized to enhance the electrochemical performance of various electrode materials of low electronic conductivity [17–20]. In the present paper, the newly suggested simple method that uses soluble methylcellulose both as a carbon source and as a dispersing agent is used for the synthesis of $Li_2FeP_2O_7$/C [21].

The structural, microstructural and electrochemical properties of the powders obtained with and without methylcellulose are compared.

2. Experimental

2.1. Materials preparation

The synthesis of carbon-free $Li_2FeP_2O_7$ (denoted as LFP) was conducted through the precipitation of an aqueous solution, followed by a thermal treatment. The aqueous solutions of $LiNO_3$, $FeSO_4 \cdot 7H_2O$, and $(NH_4)_2HPO_4$ were mixed in this order in the 2:1:2 molar ratio. The obtained precipitated solution was slowly evaporated to dryness and the precipitate was annealed for 6 hours at 600 °C under a slightly reductive atmosphere (Ar + 10%H_2). Similarly, the preparation of the $Li_2FeP_2O_7$/C composite started from the same aqueous solutions with addition of soluble methylcellulose serving both as a dispersing agent and as a carbon source (the procedure is described in detail in our previous study on the Li_2FeSiO_4/C composite [21]). The obtained powder will hereinafter be referred to as the LFP/C sample.

2.2. Materials characterization

X-ray diffraction data were collected on a Philips PW 1050 diffractometer with Cu-K$\alpha_{1,2}$ radiation (Ni filter) at a room temperature. Measurements were done in the 2θ range of 10–110° with a scanning step width of 0.02° and 14 s times per step. Crystal structure refinement was based on the Rietveld full profile method [22] using the Koalariet computing program [23].
The measurements of the Mössbauer effect in $Li_2FeP_2O_7$ powder samples were performed in transmission geometry using a ^{57}Co(Rh) source at room temperature (RT). The Wissel

spectrometer was calibrated using the spectra of natural iron foil; accordingly the isomer shift values (δ) were in reference to metallic alpha iron (δ = 0).

The carbon content in the LFP/C sample was determined by a thermal analysis of the sample using simultaneous TG–DTA (Setsys, SETARAM Instrumentation, Caluire, France) in the temperature range between 25 °C and 800 °C in air flow.

The morphology of the synthesized powders was analyzed by field emission scanning electron microscopy (FE-SEM, Supra 35 VP, Carl Zeiss).

The Fourier transform infrared (FTIR) spectra of the samples were recorded in ambient conditions in the mid-IR region (400–4000 cm^{-1}) with a Nicolet IS 50 FT-IR Spectrometer operating in the ATR mode and the measuring resolution of 4 cm^{-1} with 32 scans.

The electrical conductivity was measured at room temperature by the four-point probe DC current method on disk-shaped pellets made of pressed powders.

Electrochemical measurements were carried out in a closed, argon-filled two-electrode cell, with metallic lithium as a counter electrode. A 1M solution of $LiClO_4$ (p.a., Chemmetall GmbH) in propylene carbonate (p.a., Honeywell) was used as an electrolyte. Working electrodes were made from the synthesized material, carbon black and polyvinylidene fluoride (PVdF, Aldrich) mixed in the 75:20:5 weight percent ratio and deposited on platinum foils from the slurry prepared in N-methyl-2-pyrrolidone. Galvanostatic charge/discharge tests were performed within the potential range of 2.8 and 4.0 V at different current rates. Electrochemical impedance spectroscopy was performed in the frequency range from 10^{5}–10^{-2} Hz at an amplitude of 5 mV and a cell potential of 3.2 V (vs. Li/Li^{+}). The measurements were conducted using a Vertex.One.EIS potentiostat/galvanostat with an impedance analyzer (Ivium Technologies B.V.).

3. Results and Discussion

3.1. Morphology studies

The morphology of the synthesized powders was determined by FESEM (Figure 1). The powders looked like large crystalline masses with particles reaching several micrometres in size. The particles were highly agglomerated and sintered, with no clearly visible boundaries among them. The LFP/C powder displayed a wider particle size distribution than the LFP powder, with smaller particles among large crystalline masses.

3.3. XRD analysis

The crystal structure of the synthesized powders was confirmed by X-ray powder diffraction. The powders contained two crystalline phases: $Li_2FeP_2O_7$ as the major phase and olivine-type $LiFePO_4$ as a minor phase with the same share in both powders. The formation of $LiFePO_4$ may have been accompanied with the emergence of lithium phosphates, probably in the amorphous state. There was no evidence of the formation of crystalline carbon and the internal carbon in the LFP/C powder can be assumed to be a contribution to the background. The amount of the *in situ* formed carbon, established by a thermogravimetric analysis, was found to be 10 wt%. A two-phase refinement was performed on XRD data to quantify the amount of both $Li_2FeP_2O_7$ and $LiFePO_4$ phases, as they were both electrochemically active. Both the observed and calculated XRD patterns are given in Figure 2. The structure of $LiFePO_4$ was refined in the orthorhombic space group *Pnma* (No. 62) in the olivine type. The structure of $Li_2FeP_2O_7$ was refined in the monoclinic space group $P2_1/c$ (No. 14) in a structure type where Li^+, Fe^{2+}, P^{5+} and O^{2-} ions occupied 24 nonequivalent general 4*e* crystallographic positions [x,y,z]. P^{5+} and O^{2-} ions fully

occupied 4 and 14 positions of these 24 crystallographic positions, respectively. On the other hand, Fe^{2+} ions fully occupied one crystallographic position (denoted as Fe1) and Li^{+} ions fully occupied three crystallographic positions (denoted as Li1, Li2, and Li3). The remaining two crystallographic positions were partially occupied by both Fe^{2+} and Li^{+} ions (anti-site defect). These sites, labelled as Fe2/Li5 and Fe3/Li4, were completely occupied and had right trigonal-bipyramidal and oblique trigonal-bipyramidal (very close to tetragonal pyramidal) oxygen surrounding, respectively (Figure 3). Due to a significant difference in the X-ray scattering factors of iron and lithium ions, it was possible to refine the occupancy of iron in the mixed-occupied sites accurately. The refined values of the atomic coordinates are given in Table 1. The results of the refinements (Table 2) showed that the *in situ* formation of carbon led both to an increase of the lattice parameters and a decrease of the crystallite size (240 and 164 nm for LFP and LFP/C, respectively). Smaller primitive cell volume of LFP powder (1034.0 vs. 1035.8 $Å^3$) accompanied with larger crystallite size suggests that it constitutes more stable structure. The amount of the olivine phase was somewhat greater in the LFP/C powder (9.3 vs. 8.7 wt.% in LFP powder), implying that a more reductive atmosphere, created during the pyrolysis of methylcellulose, facilitated $LiFePO_4$ formation. This is also documented in the literature [16]. In both powders, the Fe2/Li5 mixed-occupied site was to a greater degree occupied by iron ions than the Fe3/Li4 site (0.85/0.15 and 0.71/0.29 for LFP and LFP/C, respectively). In addition, the observed different partial occupancy of the mixed-occupied sites (expressed as the Fe2/Fe3 ratio in Table 2) may be relevant for the study of lithium diffusion. Namely, Li-diffusion pathways involve conventional vacancy hopping between all neighbouring Li positions along each of the three principal axes [6]. The pyrophosphates without partial occupation have continuous, but not interconnected, two-dimensional Li^{+} ion pathways along the *bc*- plane (Figure 2). The Fe2/Li5

sites in pyrophosphates with lithium occupancy (green polyhedra in Figure 3) can connect these two-dimensional Li^+ layers, thereby mediating Li-ion diffusion [7]. It may also be assumed that the iron occupancy of the Fe3/Li4 site can interrupt the continuous pathways of Li^+ within a two-dimensional Li^+ layer, affecting Li^+ diffusion.

3.4. Mössbauer spectroscopy

The Mössbauer spectra were examined using the WinNormos-Site software package based on the least squares method [24]. The two spectra consisted of three conspicuous paramagnetic doublets, plus one doublet with an almost negligible area relative to them, see Figure 4. The fitted Mössbauer hyperfine parameters are given in Table 3.

The three main doublets in both samples came from three various Fe environments in the $Li_2FeP_2O_7$ phase (Fe1, Fe2, and Fe3 sites). According to the measured δ, every Fe ion had the 2+ valence state with a high-spin electron configuration ($t^4_{2g}e^2_g$) [25]. There was no evidence of the presence of Fe^{3+} in either investigated sample. The Fe1 was surrounded by six oxygen anions making an octahedron. As Fe1 had the largest coordination number compared to the other Fe sites, we assigned to it the doublet with the largest isomer shift value (1.27 mms^{-1}) [13,25]. This doublet also covered the highest normalized relative area, as expected for a fully occupied Fe1 position. This was the case in both samples. The line width (Γ) of 0.43 mms^{-1} (0.41 mms^{-1} in the case of LFP/C) was the consequence of a random arrangement of the next-nearest-neighbourhood (NNN). Namely, the oxygen anions of the surrounding octahedron of Fe1 were connected to one Fe2/Li5 site and one Fe3/Li4 site. The occupation of these sites with various combinations of Li and Fe ions caused small changes in the charge distribution around Fe1 ions, which was reflected in a greater line width.

The other two doublets were assigned to the mixed-occupied FeO_5 sites (Fe2 and Fe3). Their identification was difficult due to the lack of accurate calculations of the hyperfine parameters. In several published papers only one doublet was ascribed to the combination of FeO_5 sites [8, 13, 26]. Taking into consideration the partial occupancy of the mixed-occupied sites established by the Rietveld refinement and the ratio of the relative areas of these two doublets (Table 3), we ascribed the doublet with the largest area, and also with a larger isomer shift and quadrupole splitting, to the Fe2 site. There are different oxygen surroundings around the Fe2 and Fe3 sites (right trigonal-bipyramidal and oblique trigonal-bipyramidal, respectively, see Figure 2), as well as different arrangements of the next-nearest-neighbours (NNN). The right trigonal-bipyramidal surrounding enabled a greater deviation of the charge symmetry around the Fe nucleus than the oblique trigonal-bipyramidal arrangement. Therefore, the Fe2 doublet had larger quadrupole splitting, which is similar to the findings of Blidberg et al. [27]. The greater isomer shift of the Fe2 doublet was a consequence of a larger 3d population. A larger electron density led to a greater shielding of the 3s electrons by 3d, decreasing the charge density at the nucleus [25]. The ratios of the relative areas of the Fe2 doublet versus the Fe3 doublet revealed that ~ 69% and 59% of the Fe2 site was occupied by Fe^{2+} ions in the LFP and LFP/C powders, respectively. These findings were in accordance with the results of the Rietveld refinement with a slight discrepancy of the absolute values (Table 2). It is possible to estimate the relative site quantity based on the relative area of the Mössbauer subspectrum if the corresponding recoil-less factor is known. Neither in the present study, nor in the previously published papers [13, 26], was the ratio of the fitted fractions (Fe1:(Fe2 + Fe3)) 1:1. This indicates that the recoil-less factors for these sites are not equal. Another reason for this discrepancy might be that the model of the pure Lorentz lines is not suitable at all.

The minor doublet was recognized as a response from Fe^{2+} ions at their regular M2 octahedral sites in the olivine $LiFePO_4$ (phase 2 (P2) in Table 4) [28]. There was a mismatch between the $LiFePO_4$ quantities estimated by the Mössbauer spectroscopy and by the structural refinement. The values of quadrupole splitting (Δ) lower than 2.96 mms^{-1} might indicate disorder and defects, mostly anti-site Fe^{2+} defects in the olivine phase [29]. These anti-site signals could affect some parts of the spectrum, due to which one may underestimate the total representation of the olivine-type $LiFePO_4$ amount in the sample and overestimate its presence in the other parts of the spectrum.

3.5. FTIR spectroscopy

The FTIR spectra of the two powders are quite similar, with prominent bands characteristic for $(P_2O_7)^{4-}$ anions. Multiple bands in Figure 5 indicate the typical frequencies associated with P–O–P, O–P–O, and P–O vibrations [30, 31]. In addition, the spectrum of the LFP/C powder also contains vibration at around 1600 cm^{-1} that can be related to graphitic C–C nature (G-band) of carbon [14].

3.6. Electrochemical performances

The electrochemical performances were investigated using impedance spectroscopy measurements (EIS) and galvanostatic charge/discharge cycling. The EIS measurements were performed in the discharged (lithiated) state at 3.2 V after several charge/discharge cycles. The Nyquist plots indicated diffusion-controlled charge transfer processes (Figure 6). Each plot consisted of two semicircles at high and medium frequencies that overlapped into one depressed semicircle, and an inclined line at low frequency. The impedance data were fitted with the

equivalent circuit shown in the inset of Figure 6. The equivalent circuit scheme included: resistor Rs, resistor R1 paralleled with the constant phase element Q1, and resistor R_{ct} in serial with the general Warburg impedance Z_W and paralleled with the constant phase element Q2. Rs resistor was the electrolyte resistance, the second part of the equivalent circuit was related to the contact resistance between the electrode composite material and the metallic substrate (Pt) coupled in parallel with the double-layer capacitance created at the metallic substrate [32], while the third part of the equivalent circuit was related to the charge transfer resistance and Li^+ solid-phase diffusion [33]. The inclusion of the constant phase elements in the equivalent circuit, instead of the capacitors, ensured a better fitting to the experimental data. The constant phase element (CPE) has an impedance $Z = (Q(i\omega)^n)^{-1}$, $n \leq 1$, and it is frequently used to model the presence of the time-constant distributions that can arise from surface heterogeneity, geometry-induced nonuniform current and potential distributions, changes in the conductivity of oxide layers, electrode porosity or surface roughness [34]. In this case, the use of CPE, was physically reasonable keeping in mind the electrodes' preparation. The fitted parameters of the equivalent circuit are given in Table 4. The LFP/C electrode had a significantly smaller charge-transfer resistance of particle/electrolyte interfaces and a slightly larger Warburg impedance (Z_W) than the LFP electrode. Apparently, the *in situ* formed carbon enabled the reduction of crystallite sizes and provided a more conductive network; both factors lowered the charge-transfer resistance, thereby facilitating electron transfer. As the percentage of the $LiFePO_4$ phase in the two powders is similar, the differences in the Warburg impedance can be ascribed to the $Li_2FeP_2O_7$ phase, namely the different occupation of the mix-occupied sites (Table 2). A small difference between the Warburg impedances suggests that the assumed differences in the partial occupancy of the mixed-occupied site did not have a significant influence on general diffusion.

The conductivity measurements confirmed a higher conductivity of the LFP/C powder ($1.3 \cdot 10^{-6}$ Scm^{-1} vs. $0.4 \cdot 10^{-6}$ Scm^{-1}).

Figure 7 displays the discharge curves of the first cycle, as well as the delivered capacities for different current rates in the potential range of 2.8–4.0 V. The observed discharge curve profiles of the two samples consist of a slightly sloping part from 4.0–3.4 V and a plateau at 3.39 V. The sloping part originates from the $Li_2FeP_2O_7$ phase, while the plateau can be ascribed to the $LiFePO_4$ phase. In general, the carbon-containing powder exhibited a greater discharge capacity (inset of Figure 7), which decreased with an increased current rate. Moreover, the roughly estimated contribution of the existing phases ($Li_2FeP_2O_7$ and $LiFePO_4$) to the overall capacity (the sloping part and the plateau in the discharge curves) is also greater for the carbon-containing powder. This means that the *in situ* formation of carbon facilitates electron transfer (through the conductivity enhancement) in both phases – $Li_2FeP_2O_7$ and $LiFePO_4$, which typically have a low electronic conductivity.

4. Conclusions

A simple method was used for the preparation of $Li_2FeP_2O_7$ powder and its composite with carbon, $Li_2FeP_2O_7$/C. The presence of $LiFePO_4$ as a minor phase was evidenced in both powders in similar amounts. A combined X-ray diffraction and Mössbauer spectroscopy study revealed that a more reductive atmosphere, provided by the pyrolysis of methylcellulose, altered the partial occupancy by lithium of the mixed-occupied sites. Electrochemical measurements showed that the *in situ* formation of carbon, rather than different partial occupancy, increased conductivity through the reduction of the charge-transfer resistance, and enabled better lithium-

ion diffusion. The composite powder had a higher capacity that corresponded to 90% of the 1-electron theoretical capacity of the $Li_2FeP_2O_7$ phase.

Acknowledgements

The Ministry of Education, Science and Technological Development of the Republic of Serbia provided financial support for this study under Grants Nos. III 45004, III 45015, and ON 171001, and the Bilateral Cooperation Project between the Republic of Slovenia and the Republic of Serbia “Developments of novel materials for alkaline-ion batteries”.

References

[1] A. Gutierrez, N.A. Benedek, A. Manthiram, Crystal-chemical guide for understanding redox energy variations of $M^{2+/3+}$ couples in polyanion cathodes for lithium-ion batteries, Chem. Mater. 25 (2013) 4010–4016.

[2] J.B. Goodenough, K.S. Park, The Li-ion rechargeable battery: A perspective, J. Am. Chem. Soc. 135 (2013) 1167—1176.

[3] J. Zheng, Z. Yang, P. Wang, L. Tang, C. An, Z. He, Multiple Linkage Modification of Lithium-Rich Layered Oxide $Li_{1.2}Mn_{0.54}Ni_{0.13}Co_{0.13}O_2$ for Lithium Ion Battery, ACS Appl. Mater. Interfaces. 10 (2018) 31324–31329.

[4] J. Chao Zheng, Z. Yang, Z. Jiang He, H. Tong, W. Jing Yu, J. Feng Zhang, In situ formed $LiNi_{0.8}Co_{0.15}Al_{0.05}O_2$@$Li_4SiO_4$ composite cathode material with high rate capability and

long cycling stability for lithium-ion batteries, Nano Energy. 53 (2018) 613–621.

[5] S. Nishimura, M. Nakamura, R. Natsui, A. Yamada, New lithium iron pyrophosphate $Li_2FeP_2O_7$ as 3.5 V class cathode material for lithium-ion battery, JACS Commun. 132 (2010) 13596–13597.

[6] J.M. Clark, S. Nishimura, A. Yamada, M.S. Islam, High-voltage pyrophosphate cathode: Insights into local structure and lithium-diffusion pathways, Angew. Chemie - Int. Ed. 51 (2012) 13149–13153.

[7] S. Lee, S.S. Park, Structure, defect chemistry, and lithium transport pathway of lithium transition metal pyrophosphates ($Li_2MP_2O_7$, M: Mn, Fe, and Co): Atomistic simulation study, Chem. Mater. 24 (2012) 3550–3557.

[8] P. Barpanda, G. Rousse, T. Ye, C.D. Ling, Z. Mohamed, Y. Klein, A. Yamada, Neutron diffraction study of the Li-ion battery cathode $Li_2FeP_2O_7$, Inorg. Chem. 52 (2013) 3334–3341.

[9] J. Du, L. Jiao, Q. Wu, Y. Liu, Y. Zhao, L. Guo, Y. Wang, H. Yuan, Synthesis and characterization of $Li_2FeP_2O_7$/C nanocomposites as cathode materials for Li-ion batteries, Electrochim. Acta. 103 (2013) 219–225.

[10] B. Zhang, X. Ou, J.C. Zheng, C. Shen, L. Ming, Y.D. Han, J.L. Wang, S.E. Qin, Electrochemical properties of $Li_2FeP_2O_7$ cathode material synthesized by using different lithium sources, Electrochim. Acta. 133 (2014) 1–7.

[11] J.C. Zheng, X. Ou, B. Zhang, C. Shen, J.F. Zhang, L. Ming, Y.D. Han, Effects of Ni^{2+} doping on the performances of lithium iron pyrophosphate cathode material, J. Power Sources. 268 (2014) 96–105.

[12] J. Zheng, B. Yang, X. Wang, B. Zhang, H. Tong, W. Yu, J. Zhang, Comparative

investigation of $Na_2FeP_2O_7$ sodium insertion material synthesized by using different sodium sources, ACS Sustain. Chem. Eng. 6 (2018) 4966–4972.

[13] N. V. Kosova, A.M. Tsapina, A.B. Slobodyuk, S.A. Petrov, Structure and electrochemical properties of mixed transition-metal pyrophosphates $Li_2Fe_{1-y}Mn_yP_2O_7$ ($0 \leq y \leq 1$), Electrochim. Acta. 174 (2015) 1278–1289.

[14] P. Barpanda, T. Ye, S.-C. Chung, Y. Yamada, S. Nishimura, A. Yamada, Eco-efficient splash combustion synthesis of nanoscale pyrophosphate ($Li_2FeP_2O_7$) positive-electrode using Fe(III) precursors, J. Mater. Chem. 22 (2012) 13455–13459.

[15] J. Xu, S.L. Chou, Q.F. Gu, M.F. Md Din, H.K. Liu, S.X. Dou, Study on vanadium substitution to iron in $Li_2FeP_2O_7$ as cathode material for lithium-ion batteries, Electrochim. Acta. 141 (2014) 195–202.

[16] H. Jang, I. Taniguchi, Influence of impregnated carbon on preparation and electrochemical properties of $Li_2FeP_2O_7$ composite synthesized by spray pyrolysis, J. Alloys Compd. 709 (2017) 557–565.

[17] A. Eftekhari, $LiFePO_4$/C nanocomposites for lithium-ion batteries, J. Power Sources. 343 (2017) 395–411.

[18] X. Shen, Z. Tian, R. Fan, L. Shao, D. Zhang, G. Cao, L. Kou, Y. Bai, Research progress on silicon/carbon composite anode materials for lithium-ion battery, J. Energy Chem. 27 (2018) 1067–1090.

[19] P. Dhaiveegan, H.-T. Peng, M. Michalska, Y. Xiao, J.-Y. Lin, C.-K. Hsieh, (2018). Investigation of carbon coating approach on electrochemical performance of $Li_4Ti_5O_{12}$/C composite anodes for high-rate lithium-ion batteries, J. Solid State Electrochem. 22 (2018) 1851–1861.

[20] J. Zheng, Y. Han, D. Sun, B. Zhang, E.J. Cairns, In situ-formed $LiVOPO_4@V_2O_5$ core-shell nanospheres as a cathode material for lithium-ion cells, Energy Storage Mater. 7 (2017) 48–55.

[21] M. Milović, D. Jugović, M. Mitrić, R. Dominko, I. Stojković-Simatović, B. Jokić, D. Uskoković, The use of methylcellulose for the synthesis of Li_2FeSiO_4/C composites, Cellulose. 23 (2016) 239–246.

[22] H.M. Rietveld, A profile refinement method for nuclear and magnetic structures, J. Appl. Crystallogr. 2 (1969) 65–71.

[23] R.W. Cheary, A. Coelho, A fundamental parameters approach to X-ray line-profile fitting, J. Appl. Crystallogr. 25 (1992) 109–121.

[24] R.A. Brand, WinNormos Mössbauer fitting program, Universität Duisburg, 2008.

[25] F. Menil, Systematic trends of the ^{57}Fe Mössbauer isomer shifts in (FeO_n) and (FeF_n) polyhedra. Evidence of a new correlation between the isomer shift and the inductive effect of the competing bond T-X (→ Fe) (where X is O or F and T any element with a formal positive charge), J. Phys. Chem. Solids. 46 (1985) 763–789.

[26] N. Furuta, S.-I. Nishimura, P. Barpanda, A. Yamada, Fe^{3+}/Fe^{2+} redox couple approaching 4V in $Li_{2-x}(Fe_{1-y}Mn_y)P_2O_7$ pyrophosphate cathodes, Chem. Mater. 24 (2012) 1055–1061.

[27] A. Blidberg, L. Häggström, T. Ericsson, C. Tengstedt, T. Gustafsson, F. Björefors, Structural and electronic changes in $Li_2FeP_2O_7$ during electrochemical cycling, Chem. Mater. 27 (2015) 3801–3804.

[28] R. Amisse, M.T. Sougrati, L. Stievano, C. Davoisne, G. Dražič, B. Budič, R. Dominko, C. Masquelier, Singular structural and electrochemical properties in highly defective $LiFePO_4$ powders, Chem. Mater. 27 (2015) 4261–4273.

[29] A.S. Andersson, B. Kalska, L. Haggstrom, J.O. Thomas, Lithium extraction/insertion in $LiFePO_4$: An X-ray diffraction and Mössbauer spectroscopy study, Solid State Ionics. 130 (2000) 41–52.

[30] H. Bih, I. Saadoune, H. Ehrenberg, H. Fuess, Crystal structure, magnetic and infrared spectroscopy studies of the $LiCr_yFe_{1-y}P_2O_7$ solid solution, J. Solid State Chem. 182 (2009) 821–826.

[31] H. Kim, S. Lee, Y. Park, H. Kim, J. Kim, S. Jeon, K. Kang, Neutron and X-ray diffraction study of pyrophosphate-based $Li_{2-x}MP_2O_7$ (M = Fe , Co) for lithium rechargeable battery electrodes, Chem. Mater. 23 (2011) 3930–3937.

[32] M. Gaberscek, J. Moskon, B. Erjavec, R. Dominko, J. Jamnik, The importance of interphase contacts in Li ion electrodes: The meaning of the high-frequency impedance arc, Electrochem. Solid-State Lett. 11 (2008) A170–A174.

[33] J.-M. Atebamba, J. Moskon, S. Pejovnik, M. Gaberscek, On the interpretation of measured impedance spectra of insertion cathodes for lithium-ion batteries, J. Electrochem. Soc. 157 (2010) A1218–A1228.

[34] M.E. Orazem, B. Tribollet, Electrochemical impedance spectroscopy, John Wiley & Sons, Inc., Hoboken, New Jersey, 2008.

Table 1. Refined fractional atomic coordinates and their estimated standard deviations.

sample	$Li_2FeP_2O_7$/C			$Li_2FeP_2O_7$	
atom	x	y	z	x	y
Fe1	0.673(2)	0.568(1)	0.698(2)	0.678(2)	0.568(2)
Fe2	0.829(2)	0.273(2)	0.759(2)	0.830(2)	0.277(2)
Fe3	0.074(1)	0.082(2)	0.686(2)	0.064(1)	0.0767(2)
P1	0.575(2)	0.658(2)	0.381(3)	0.582(3)	0.655(3)
P2	0.262(2)	0.593(3)	0.578(3)	0.255(2)	0.570(3)
P3	0.897(2)	0.814(3)	0.609(3)	0.895(2)	0.815(3)
P4	0.729(3)	0.049(3)	0.527(3)	0.741(3)	0.040(3)
O1	0.829(4)	0.214(5)	0.593(5)	0.827(4)	0.210(5)
O2	0.762(5)	0.024(6)	0.458(6)	0.774(5)	0.023(5)
O3	0.378(5)	0.563(6)	0.985(5)	0.373(5)	0.588(6)
O4	0.143(4)	0.556(5)	0.616(5)	0.149(4)	0.558(5)
O5	0.667(4)	0.301(5)	0.341(5)	0.713(4)	0.332(5)
O6	0.732(5)	0.423(6)	0.555(5)	0.729(4)	0.418(6)
O7	0.039(4)	0.266(6)	0.012(5)	0.047(4)	0.273(5)
O8	0.427(4)	0.291(5)	0.185(5)	0.398(4)	0.291(5)
O9	0.831(4)	0.637(5)	0.684(4)	0.844(4)	0.639(5)
O10	-0.006(4)	0.866(4)	0.682(5)	-0.018(5)	0.853(4)
O11	0.473(4)	0.888(5)	0.770(5)	0.493(4)	0.911(5)
O12	0.578(5)	0.667(5)	0.543(6)	0.567(5)	0.686(5)
O13	0.251(4)	0.053(6)	0.079(5)	0.244(5)	0.057(6)
O14	0.214(5)	0.098(5)	0.401(5)	0.211(5)	0.101(5)
Li1	0.525(17)	0.406(17)	0.120(19)	0.598(22)	0.506(27)
Li2	0.681(15)	0.656(14)	0.223(20)	0.723(14)	0.586(17)
Li3	0.557(18)	0.506(19)	-0.044(22)	0.391(24)	0.527(29)
Li4	= Fe3	= Fe3	= Fe3	= Fe3	= Fe3
Li5	= Fe2	= Fe2	= Fe2	= Fe2	= Fe2

Table 2. The main parameters of the Rietveld structural refinement.

Sample	LFP	LFP/C
Lattice parameters /Å	a = 11.0229(7) b = 9.7581(6) c = 9.8111(5) β = 101.521(4)°	a = 11.0317(9) b = 9.7616(7) c = 9.8163(6) β = 101.529(4)°
Primitive cell volume /Å^3	1034.0(1)	1035.8(1)
Crystallite size /nm	240(9)	164(5)
Fe2/Fe3 iron partial occupancy	0.85(2)/0.15	0.71(2)/0.29
Weight percent of $LiFePO_4$ /%	8.7(2)	9.3(1)
R_{wp} factor /%	2.62	2.23

Table 3. The fitted Mössbauer hyperfine parameters at a room temperature.[a]

Sample	Phase	Site	*A*/ %	A_p/ %	*Γ*/ mms^{-1}	*δ*/ mms^{-1}	*Δ*/ mms^{-1}
LFP	P1	$Fe_1^{2+\ o}$	43(7)	44.3	0.43(1)	1.27(3)	2.18(6)
		$Fe_2^{2+\ tb}$	37(10)	38.2	0.36(2)	1.225(4)	2.56(3)
		$Fe_3^{2+\ tb}$	17(9)	17.5	0.27(5)	1.128(8)	2.17(2)
	P2	$Fe_{M2}^{2+\ o}$	3(1)		0.21*	1.201(8)	2.94(2)
LFP/C	P1	$Fe_1^{2+\ o}$	50(6)	52.1	0.41(1)	1.27(1)	2.16(3)
		$Fe_2^{2+\ tb}$	27(7)	28.1	0.32(2)	1.221(3)	2.58(2)
		$Fe_3^{2+\ tb}$	19(6)	19.8	0.26(3)	1.123(7)	2.17(2)
	P2	$Fe_{M2}^{2+\ o}$	4(1)		0.21*	1.218(6)	2.95(1)

[a]*A*- relative area of subspectrum; A_p- the relative area within the $Li_2FeP_2O_7$ phase; *Γ*- line width; *δ* - measured isomer shift; Δ-quadrupole splitting. Identified phases: P1 - $Li_2FeP_2O_7$ and P2 - $LiFePO_4$. Site designation: o- completely filled FeO_6 octahedral site, tb - partially filled FeO_5 trigonal-bipyramidal site. The fitting errors are presented in parenthesis, while asterisk denotes the fixed value of linewidth.

Table 4.The kinetic parameters obtained from the fitting of the electric equivalent circuit to the experimental data.

sample	LFP	LFP/C
Rs /Ω	71.67	61.91
Rct /Ω	422.7	121.3
Zw /Ω $s^{-½}$	32.60	33.15

Figure captions

Figure 1. FESEM micrographs of LFP (a, b) and LFP/C (c,d).

Figure 2. The observed (·), calculated (-), and the difference between the observed and calculated (bottom) X-ray diffraction data taken at a room temperature of a) LFP and b) LFP/C powders. Vertical markers below the diffraction patterns indicate positions of possible Bragg reflections for monoclinic $Li_2FeP_2O_7$ (upper) and for olivine-type $LiFePO_4$ (lower).

Figure 3. The arrangement of lithium polyhedra in a monoclinic $Li_2FeP_2O_7$ structure viewed along the *c*-axis.

Figure 4. The Mössbauer spectra at T = 294 K of a) LFP and b) LFP/C. The experimental data are presented by solid circles and the fit is given by the red solid line. Vertical arrow denotes relative position of the lowermost peak with a respect to the basal line (relative transmission). The fitted lines of subspectra are plotted above the main spectrum fit the Fe1 doublet (olive), the Fe2 doublet (cyan), the Fe3 doublet (blue), and the $LiFePO_4$ (orange). The error is depicted as the difference (Th-Exp). The largest value of the absolute difference is less than a) 0.18% and b) 0.14%.

Figure 5. FTIR spectra of LFP (red) and LFP/C (blue).

Figure 6. The Nyquist plots of LFP (red) and LFP/C (blue) and the equivalent circuit scheme used for the EIS analysis.

Figure 7. The discharge curves of LFP (red dashed line) and LFP/C (blue solid line) at different current rates and the rate performance (inset).

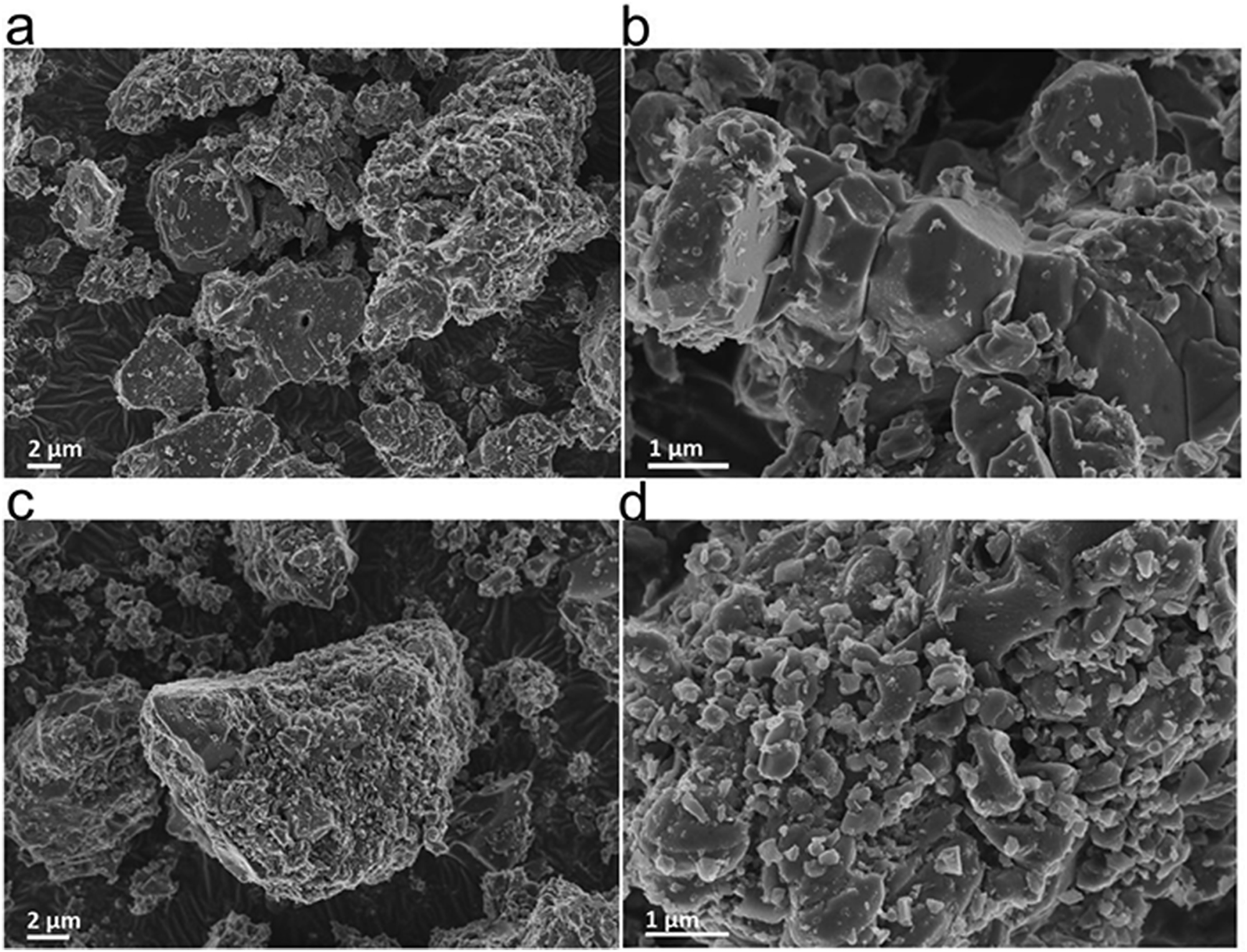
a
2 µm
b
1 µm
c
2 µm
d
1 µm

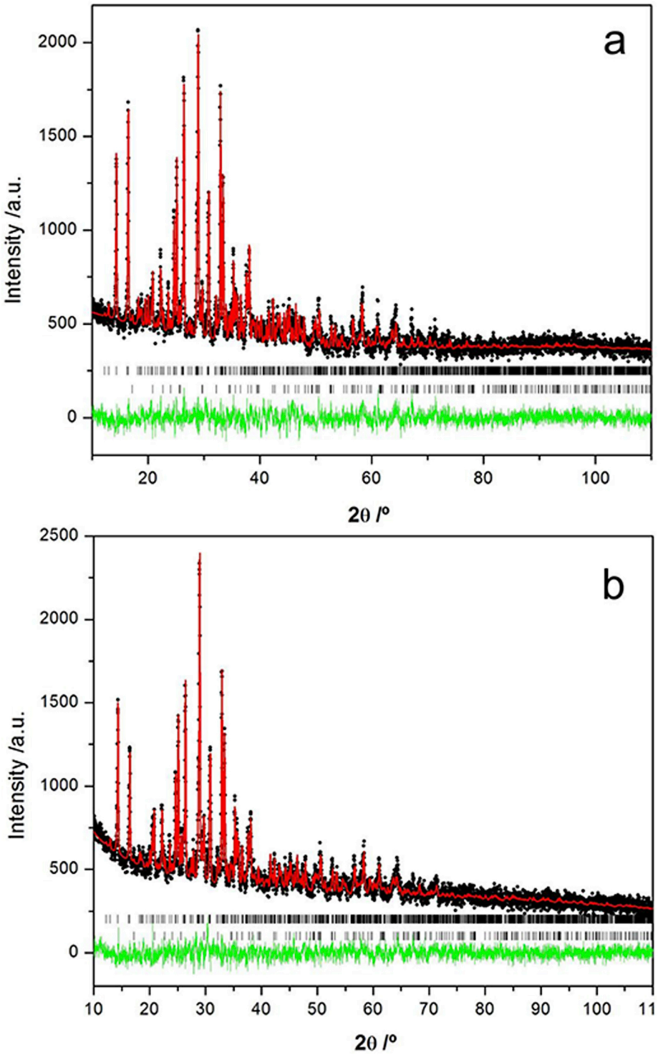
a
Intensity /a.u.
2000
1500
1000
500
0
20
40
60
80
100
2θ /°
b
Intensity /a.u.
2500
2000
1500
1000
500
0
10
20
30
40
50
60
70
80
90
100
11
2θ /°

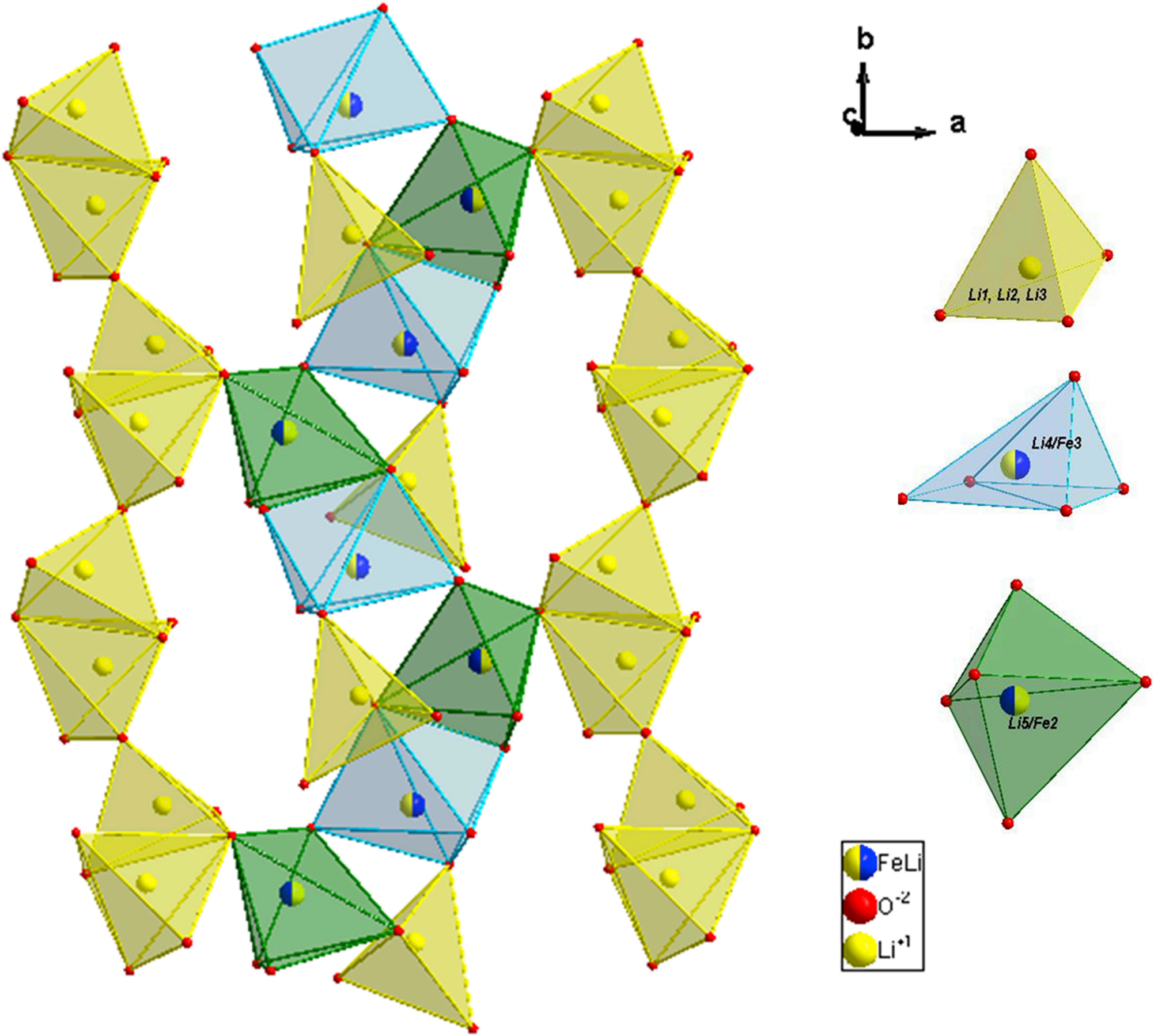
b
c
a
Li1, Li2, Li3
Li4/Fe3
Li5/Fe2
FeLi
O-2
Li+1

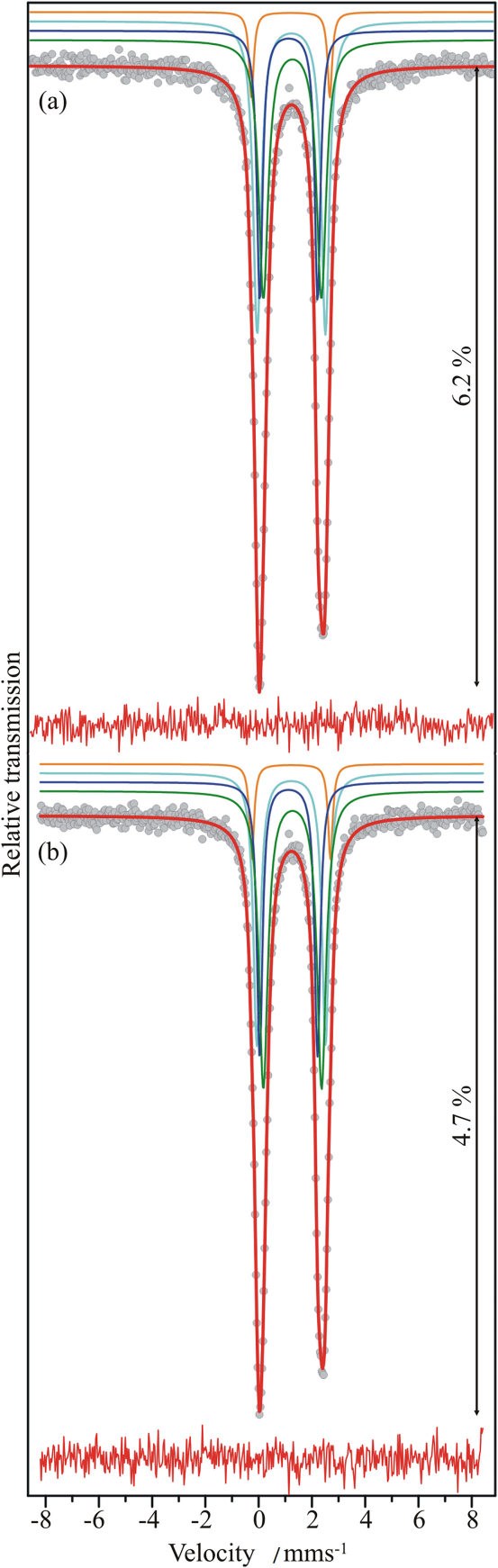
(a)
6.2 %
(b)
4.7 %
Relative transmission
-8
-6
-4
-2
0
2
4
6
8
Velocity /mms-1

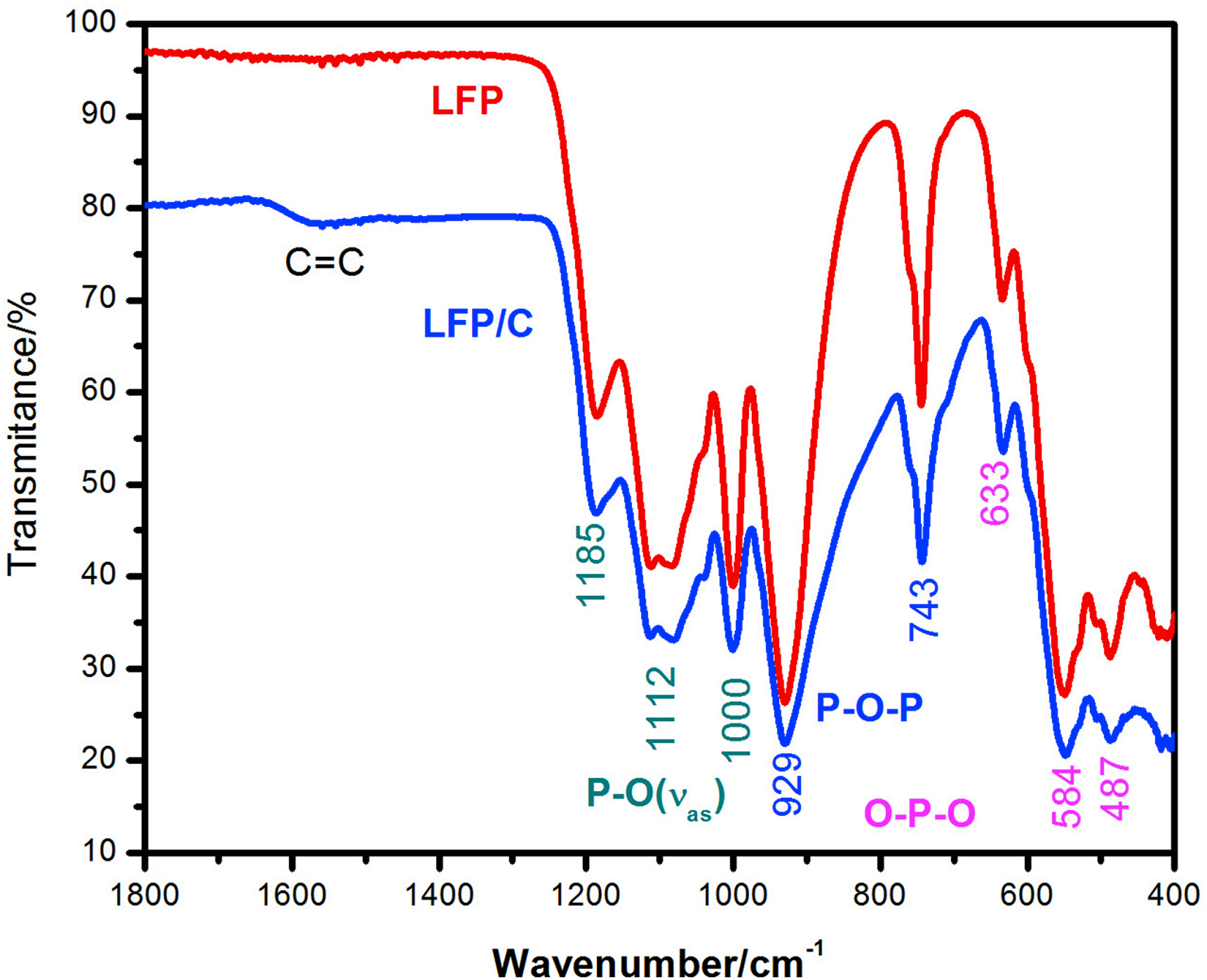
LFP
C=C
LFP/C
1185
1112
1000
929
743
633
584
487
P-O(ν as)
P-O-P
O-P-O
Transmitance/%
Wavenumber/cm-1
100
90
80
70
60
50
40
30
20
10
1800
1600
1400
1200
1000
800
600
400

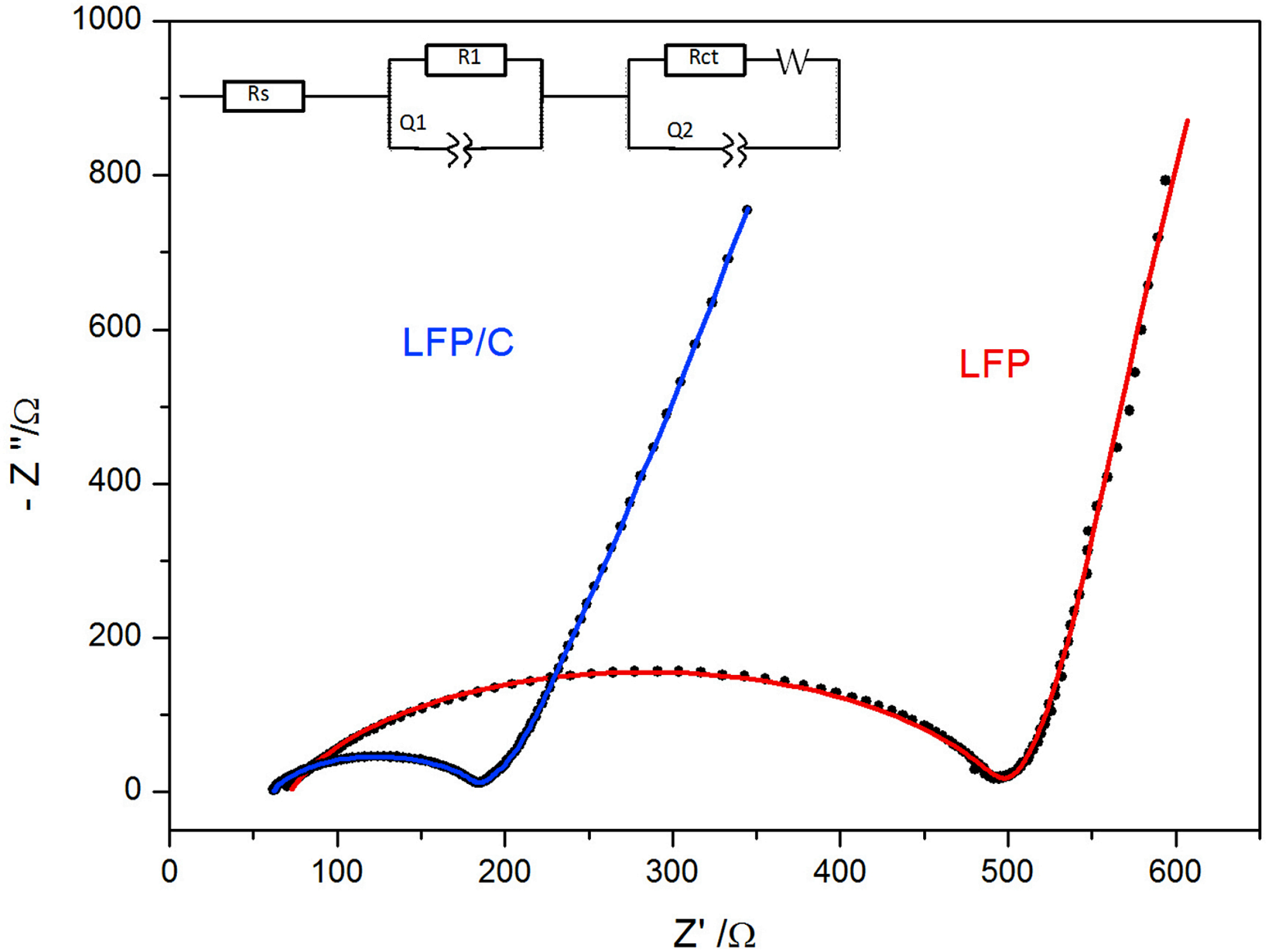
Rs
R1
Q1
Rct
W
Q2
LFP/C
LFP
- Z ''/Ω
Z' /Ω
0
200
400
600
800
1000
0
100
200
300
400
500
600

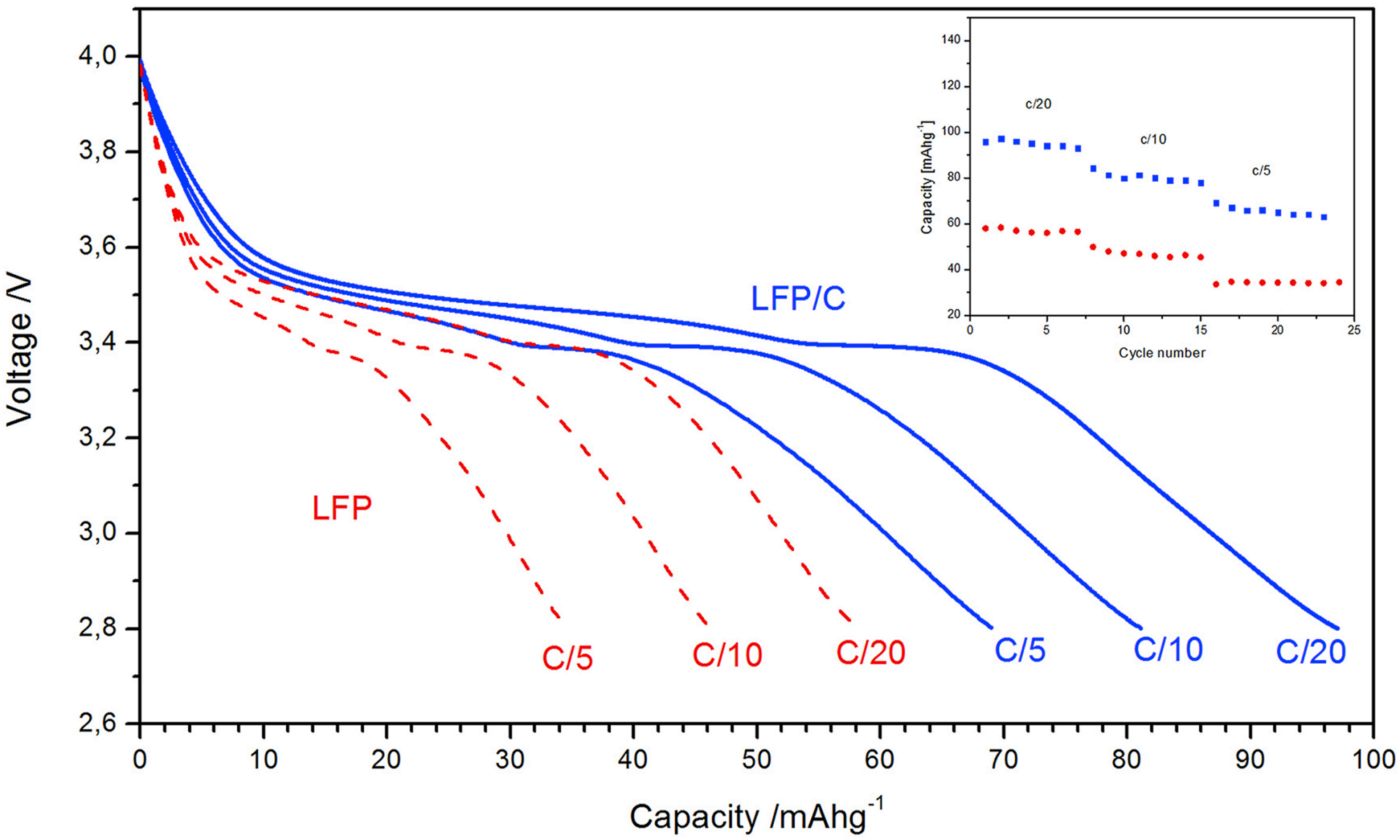
Voltage /V
4,0
3,8
3,6
3,4
3,2
3,0
2,8
2,6
0
10
20
30
40
50
60
70
80
90
100
Capacity /mAhg-1
LFP/C
LFP
C/5
C/10
C/20
C/5
C/10
C/20
Capacity [mAhg-1]
140
120
100
80
60
40
20
0
5
10
15
20
25
Cycle number
c/20
c/10
c/5

- Methylcellulose matrix is used for the synthesis of $Li_2FeP_2O_7$ and carbon composite.
- The formation of carbon altered the partial occupancy of the mixed-occupied sites.
- Increased conductivity due to the reduction of the charge-transfer resistance.